Available online at www.sciencedirect.com

SciVerse ScienceDirect

Ceramics International 39 (2013) 3249–3259

CERAMICS INTERNATIONAL

www.elsevier.com/locate/ceramint

The effect of cation type, intergranular phase amount and cation mole ratios on z value and intergranular phase crystallization of SiAlON ceramics

Nurcan Calis Acikbas*, Oguzhan Demir

Department of Mechanical and Manufacturing Engineering, Bilecik S.E. University, Bilecik, Turkey

Received 31 August 2012; received in revised form 5 September 2012; accepted 1 October 2012
Available online 11 October 2012

Abstract

The chemical resistance of SiAlONs is controlled by various factors such as z value, microstructure, type and amount of sintering additives, and intergranular phase nature (amorphous or crystalline). In this study, the relationship between z value and intergranular phase crystallization of α':β'-SiAlON composites reinforced with TiN (17 wt%) was investigated by using various dopant systems (Y:Sm:Ca, Yb:Sm:Ca, and Er:Sm:Ca) and various amounts of intergranular phase. The effect of TiN on densification, phase assemblage and microstructural evolution of composites was systematically investigated. Further, the effects of variations in the sintering aid amount and cation mole ratios on density, hardness and fracture toughness were determined in relation to z values. It was found that high z value (>0.5), crystalline intergranular phase and appropriate mechanical properties can be achieved by selecting the type of sintering additive, its amount and ratio.

Keywords: B. Composites; C. Mechanical properties; D. SiAlON; z Value

1. Introduction

SiAlON ceramics are candidate materials for structural applications both at ambient and elevated temperatures due to their excellent combination of mechanical, thermal and chemical properties [1,2]. These materials possess high wear and chemical resistance at high temperatures for a number of engineering applications. For example, SiAlON cutting tools are most extensively used in cast iron machining. However, their fracture toughness and chemical wear resistance are slightly inferior when compared to commercial Al_2O_3–SiCw cutting tools, which are used in super alloy machining. The addition of hard particles like TiN to silicon nitride based ceramic matrix is a possible way to improve the toughness and chemical wear resistance [1,2]. Apart from toughness and chemical wear resistance improvement, TiN addition can enhance Si_3N_4 strength up to 1000 MPa [3]. Hence it is expected that TiN reinforced SiAlONs are the promising candidates for cutting tool applications.

The sinterability of SiAlONs is better than that of Si_3N_4 as the presence of oxygen facilitates densification of SiAlONs. It is well known that the chemical resistance of SiAlONs is controlled by its composition, microstructure, type and amount of sintering additives, intergranular phase chemistry (amorphous or crystalline) and z value (Al–O substitution in β-Si_3N_4 crystal lattice, $\beta' = Si_{6-z}Al_zO_zN_{8-z}$). The low z SiAlON ceramics exhibit better mechanical properties like β-Si_3N_4 ceramics, whilst high z SiAlONs have properties resembling that of Al_2O_3 ceramics (good chemical resistance). Previous studies showed that z value is a very effective parameter on wear resistance, thermal sock resistance, mechanical strength, hardness, fracture toughness, creep resistance, corrosion resistance, Young's modulus, densification and machining performance of SiAlON ceramics [4–15].

Briefly, based on the existing literature it can be stated that increase in z value improves corrosion resistance [4],

*Corresponding author. Tel.: +90 228 214 1540; fax: +90 228 214 12 22.
E-mail addresses: nurcan.acikbas@bilecik.edu.tr, ncalis@gmail.com (N. Calis Acikbas).

0272-8842/$ - see front matter © 2012 Elsevier Ltd and Techna Group S.r.l. All rights reserved.
http://dx.doi.org/10.1016/j.ceramint.2012.10.013

wear resistance [5,8,9,13], increases grain size [11], provides easier densification [10,12] and reduces Young's modulus [4,7], deteriorate creep resistance [4], thermal shock resistance [5,6], strength [7,10,14], fracture toughness [7,9,12,14] and hardness [11,12,14]. Therefore z value plays a dominant role in the determination of the chemical and mechanical properties of SiAlONs.

There has been considerable amount of research work was reported on tailoring microstructure of silicon nitride ceramics by using different types of cations such as Lu, La, Yb and others [16–22]. However, to the best of authors' knowledge the effects of the cations on the z value and relationship between the z value and the intergranular phase (IGP) crystallization have not been investigated so far. Factors such as type and nature (whether crystalline or not), melting temperature, and viscosity of the intergranular phase are all important and they can be controlled by the type of sintering additives, cation molar ratios and sintering schedule [16,17]. These factors especially govern the high temperature properties of the SiAlONs. It is known that crystallization of the intergranular phase enhances the high temperature properties of liquid phase sintered ceramics. Therefore, one of the main aspects in designing SiAlONs with improved high temperature properties would be to select a sintering additive that would provide a good liquid phase sintering behavior and at the same time it would aid the refractory phase crystallization after sintering.

There has been great progress on the studies related to the effects of the z value on density, fracture toughness, hardness, thermal shock resistance, strength, wear resistance of SiAlONs and the effects of cation types on tailoring microstructure [4–22]. However, the relationship between the z value and the intergranular phase chemistry (amorphous or crystalline) has not yet been emphasized. Our preliminary studies have shown that it was not possible to produce high z value ($z > 0.5$) SiAlONs with crystalline intergranular phase, and to the best of our knowledge, there is no related data available in the literature. Therefore z value and IGP crystallization relationship is an important subject that needs to be investigated in SiAlON ceramics production, which is necessary to improve further chemical wear resistance of SiAlONs. Both the high z value and crystalline intergranular phase may affect chemical resistance especially at high temperatures.

In the SiAlON ceramics, with an increasing fraction of amorphous intergranular phase the desired high temperature and chemical resistance properties deteriorate. For instance, crystalline intergranular phase and high z value are needed to improve further chemical and wear resistance. In order to meet such a target, TiN reinforced α':β'-SiAlONs ($25\alpha'$:$75\beta'$) has been produced by using different types of cation systems (Y:Sm:Ca, Yb:Sm:Ca, and Er:Sm:Ca), and the relationship between z value and intergranular phase chemistry was determined using various sintering aids. Additionally, the effects of varying sintering additive amount and cation mole ratios on density, hardness and fracture toughness has been analyzed and correlated to z values.

2. Materials and methods

Commercially available powders in appropriate amounts were used as starting materials to produce α':β'-SiAlON composites with TiN (17 wt%). The chemical composition of raw material for the processing of SiAlON ceramics is as follows: high purity α-Si_3N_4 powder (E-10 grade, UBE Co. Ltd., Japan) with 1.4 wt% O content, high purity AlN powder (H Type, Tokuyama Corp., Japan) containing 1.6 wt% O, Al_2O_3 (Alcoa A16-SG, Pittsburgh, USA), Y_2O_3 (> 99.9%, H.C. Starck Berlin, Germany), Er_2O_3 (> 99.99%, Treibacher, Austria), Yb_2O_3 (> 99.99%, Treibacher, Austria), Sm_2O_3 (> 99.9%, Stanford Materials Corp., USA), $CaCO_3$ (> 99.75%, Reidel-de Haen, Germany) and TiN powder with average particle size of 1–2 μm (> 99% pure, H.C. Starck, Grade C, Berlin, Germany).

It has to be noted here that Y_2O_3 and/or Re_2O_3 (where $Z_{Re} \geq 62$) were used in order to increase the stability and hardness of α'-SiAlON, Sm_2O_3 (where $Z_{Re} < 62$) was used to develop elongated β'-SiAlON grains and hence increase the fracture toughness, and CaO was used in order to avoid $\alpha \rightarrow \beta$ SiAlON transformation [23]. $25\alpha'$:$75\beta'$ SiAlON compositions were formulated which have different z values (z: 0.25, 0.7 and 1), cation systems (9Y/Er/Yb:0.5Sm:0.5Ca and 4.5Y:4.5Sm:1Ca), and additive contents (IGP mol%: 1.5, 2, 2.5 and 3.3; see Table 1). The composition of the SiAlONs in the sample with nominal $n=1.3$ and $m=1.25$ has the x value of 0.416 ($x=m/3$).

The slurries with the above compositions were prepared by wet milling in isopropyl alcohol using Si_3N_4 balls. The slurries were then dried using a rotary evaporator and sieved with a mesh size of 250 μm. The powders were uniaxially pressed to a maximum pressure of 25 MPa, and subsequently cold isostatically pressed at 300 MPa to increase the green density. The pellets were sintered using a two-step gas pressure sintering cycle with a maximum

Table 1
Designed SiAlON compositions with $25\alpha'$:$75\beta'$-SiAlON phase content.

Sample code	Cation mole content	Aimed z values	Intergranular phase content (mol%)
YZ2G2	9Y:0.5Sm:0.5Ca	0.25	2.00
YZ7	9Y:0.5Sm:0.5Ca	0.70	2.50
YZ7G2	9Y:0.5Sm:0.5Ca	0.70	2.00
YZ7G1	9Y:0.5Sm:0.5Ca	0.70	1.50
EZ7	9Er:0.5Sm:0.5Ca	0.70	2.50
EZ7G2	9Er:0.5Sm:0.5Ca	0.70	2.00
EZ7G1	9Er:0.5Sm:0.5Ca	0.70	1.50
YbZ7	9Yb:0.5Sm:0.5Ca	0.70	2.50
YbZ7G2	9Yb:0.5Sm:0.5Ca	0.70	2.00
YbZ7G1	9Yb:0.5Sm:0.5Ca	0.70	1.50
YZ10G3	4.5Y:4.5Sm:1Ca	1.00	3.30

of 2.2 MPa nitrogen gas pressure at 1890 °C for 90 min and then the furnace was allowed to cool at a rate of 5 °C/min. The archimedes principle was used to measure the density of samples after sintering. The types of crystalline phases and the α′:β′-SiAlON phase ratios were determined by means of X-ray diffraction analyses (XRD-Panalytical, Empyrean with Cu-Kα radiation).

The α′:β′-SiAlON phase ratios were found by quantitative estimation from the XRD patterns using the integrated intensities of the (102) and (210) reflections of α′-SiAlON and the (101) and (210) reflections of β′-SiAlON by the following equation:

$$\frac{I_\beta}{I_\beta + I_\alpha} = \frac{1}{1 + K[(1/w_\beta) - 1]} \quad (1)$$

where I_α and I_β are observed intensities of α′- and β′-SiAlON peaks, respectively, w_β is the relative weight fraction of β-SiAlON, and K is the combined proportionality constant resulting from the constants in the two equations, namely:

$$I_\beta = K_\beta * W_\beta \quad (2)$$

$$I_\alpha = K_\alpha * W_\alpha \quad (3)$$

which is 0.518 for β (101)–α (102) reflections and 0.544 for β (210)–α (210) reflections [24].

The cell parameters of SiAlONs were measured with silicon powders as the internal standard. The z-value of the β-SiAlON phase was obtained from the mean of the z_a and z_c values given by the following equations:

$$z_a = \frac{a - 7.6044}{0.031} \quad (4)$$

$$z_c = \frac{c - 2.9075}{0.026} \quad (5)$$

where a and c are the calculated unit cell dimensions of β-SiAlON: JCPDS card 33-1160 was used as a reference for β-Si_3N_4 where $a = 7.6044(2)$ Å and $c = 2.9075(1)$ Å.

The microstructural investigation of the polished surfaces of samples was performed by means of a scanning electron microscope (SEM-ZEISS Supra 40VP) by using back-scattered electron imaging mode. The mechanical properties, in particular hardness and indentation fracture toughness of the samples were determined by indenting the mirror polished surfaces by applying a load of 10 kg for 10 s using Vickers hardness tester. The Vickers hardness (HV) was calculated by the following equation (Evans and Charles) [25]:

$$HV10 = 0.47P/a^2 \quad (6)$$

where $HV10$ is the Vickers hardness, P is load applied and a is half the length of the diagonal of the indentation produced by the indenter. The fracture toughness (K_{IC}) has been evaluated using the indentation fracture (IF) toughness technique. In this study, the indentation fracture toughness K_{IC} (MPa $m^{1/2}$) was calculated using the appropriate formula proposed by Niihara et al. [26] for median cracks:

$$K_{IC} = 0.018HV \times a^{0.5}(E/HV)^{0.4} \times (c/a - 1)^{-0.5} \quad (for\ c/a < 3.5\ and\ l/a < 2.5) \quad (7)$$

where $2a$ is the average indent diagonal length (μm), $2c$ is the crack length (from one crack tip to another), E is the elastic modulus (GPa) which is taken as a constant equivalent to 320 GPa for all the samples and H is the measured hardness (GPa). Both the indent diagonal and crack length were carefully measured from optical images of the indented surfaces and the reported hardness and fracture toughness values are the average of at least five indentation measurements. The indentation damage behavior of materials was studied in detail using SEM.

3. Results and discussion

3.1. The effect of TiN on densification, phase assemblage and microstructural evolution

Effect of TiN addition on the densification of SiAlON compositions was investigated for YZ7, EZ7 and YbZ7 samples which have a z value of 0.7. The results of the measured densities of SiAlON and the SiAlON–TiN ceramics are presented in Table 2. The results indicate that the open porosity levels of SiAlON and SiAlON–TiN composites are comparable and it reflects that TiN addition does not adversely affect the sinterability of SiAlON. The densification behavior was observed to be similar for the samples which were doped with different types of cations. The slight weight loss increment with TiN addition was a clue that the densification of SiAlONs was facilitated. It is mainly due to the presence of a TiO_2 layer on TiN particles. From Table 2, it is evident that the samples could be sintered at about 1890 °C with a weight loss of ≥ 1 wt%.

Previously, Duan et al. [27] found that TiN additives (as a thin layer of TiO_2 present on the surface of powders) decrease the sintering temperature of Si_3N_4 and lead to the phase transformation from α- to β-Si_3N_4. They hypothesized that the presence of Ti^{4+} ions in the intergranular liquid phase decreased the viscosity, which could explain why the ratio of α- to β-Si_3N_4 was lower. Ekström and Olsson reported that β′-SiAlON–TiN composites could be sintered at a low temperature of 1650 °C, which was several hundred degrees below the required temperature for obtaining single phase β-Si_3N_4 ceramics [28].

Fig. 1 shows the effect of TiN addition on β′:α′ phase ratio and crystallization of SiAlON compositions which have similar intergranular phase content but different cation types. The phase evolution of samples after sintering with and without TiN addition showed almost similar β′:α′ phase ratios (see Table 2). Evidently, the calculated z values are in good agreement with the targeted z values in the designed YZ7, EZ7 and YbZ7 compositions, and TiN addition had no significant effect on z values. On the

Table 2
Comparison densification behavior, phase evolution and change in z values of SiAlON and SiAlON–TiN composites.

	YZ7		EZ7		YbZ7	
	None	**TiN added**	**None**	**TiN added**	**None**	**TiN added**
B.D.	3.2445	3.4813	3.3586	3.5812	3.3765	3.5927
%O.P.	0.03	0.09	0.03	0.03	0.01	0.08
%W.L.	1.43	1.56	1.17	1.32	1.65	1.70
β′:α′ (%)	83β′:17α′	81β′:19α′	79β′:21α′	81β′:19α′	75β′:25α′	81β′:19α′
Type of IGP	Amorphous	Melilite(vvw)	Melilite	Melilite	Silicate	Silicate
***z* value**	0.64	0.68	0.65	0.66	0.66	0.69

vvw: very very weak.

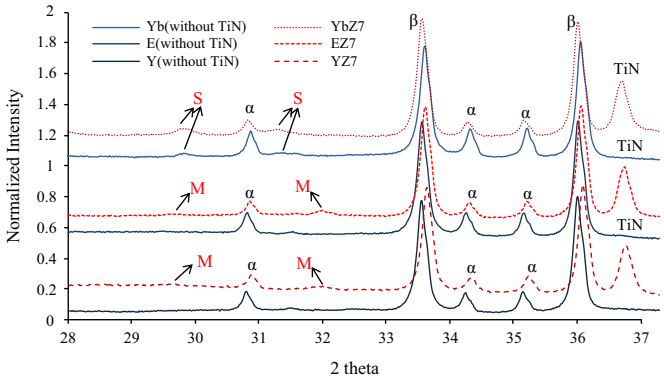

Fig. 1. Comparison of the crystallinity in 9Y/Yb/Er–0.5Sm–0.5Ca containing compositions with and without TiN (β′: beta SiAlON phase, α′: alpha SiAlON phase, M′: melilite phase ($Ln_2Si_{3-x}Al_xO_{3+x}N_{4-x}$), and S′: silicate phase ($Yb_2Si_2O_7$)).

other hand, TiN addition did not result in increase of β-SiAlON phase content. However, weak melilite peaks were observed for Y doped SiAlON after TiN addition. It indicates that TiN might have lowered liquid phase viscosity and been instrumental in the crystallization of melilite phase.

In order to compare the microstructural differences with the TiN addition, typical backscattered SEM images of 9Y:0.5Sm:0.5Ca doped SiAlON (z:0.7) and SiAlON–TiN composite are shown in Fig. 2. The microstructure of the samples reveals the presence of three different contrasting phases. The prismatic grains with darker contrast were β′-SiAlON, the equiaxed grains with lighter gray contrast were α′-SiAlON and the grains with sharp contrast were TiN due to the strong electron-scattering of the Ti atoms. The microstructures indicate no sign of agglomeration, which may be because of good dispersion of TiN particles in isopropyl alcohol. Fig. 2(a) and (b) reveals that the microstructure of the two samples appears to be very much similar, whereas TiN addition leads to the grain growth by causing the formation of more liquid phase formation which lowered the viscosity (Fig. 2d). If TiN particles were not well dispersed, the coalescence of TiN particles would have certainly shown detrimental effect on the strength and fracture toughness of the composite since microstructure would influence the mechanical properties of the material. The mechanical properties of SiAlONs will be discussed in the subsequent section.

3.2. The effect of cation type on the z value and the IGP crystallization

Table 3 presents the densification behavior of SiAlON–TiN composites which have different types of sintering additives and different amounts of IGP. It is observed that open porosity levels were similar in all samples which have different cation systems. In an earlier study, Menon and Chen [29] reported that heavier rare earths like Er and Yb can effectively wet AlN. Similar phenomenon was also reported by Hwang and Chen for Y containing system [30]. In the Y–SiAlON system, Y_2O_3–Al_2O_3–SiO_2 liquid phase preferentially wets AlN, resulting in the formation of β_{60}-SiAlON as the transient phase. Therefore wetting properties of Er, Yb and Y dopants are similar and hence they have similar densification behavior.

In order to investigate the effects of the cation types on the z value and the IGP crystallization of SiAlONs, Y, Yb and Er rich (9Y/Yb/Er:0.5Sm:0.5Ca) cation systems were used for SiAlON compositional design and z value was kept constant at 0.7. The XRD patterns for sintered samples are shown in Fig. 3. All the sintered samples showed the presence of crystalline secondary phases except for the YZ7 sample which yielded a trace of melilite phase. The slow cooling might have facilitated the crystallization of grain boundary phase during cooling. It is obvious that crystallization tendency of Er and Yb cations is higher than that of Y cation. B-type disilicate phase ($Yb_2Si_2O_7$) was observed for the YbZ7 sample, whilst melilite phase was noticed in EZ7. Mandal et al. [31,32] reported that the effect of cation radius on the oxynitride phases formed during the post sintering heat treatment of lanthanides modified Si–Al–O–N glasses. The smaller radius cations (Y, Er, etc.) disilicate or B phase was reportedly more stable. In the present case, melilite phase crystallization was observed instead of disilicate phase for YZ7 and EZ7 samples and B-type disilicate phase for the YbZ7 sample. It can be seen from the results that the disilicate phase was no longer stable when the cation size of the sintering additives was larger than 0.8697 Å (for 9Yb:0.5 Sm:0.5Ca). As the ionic

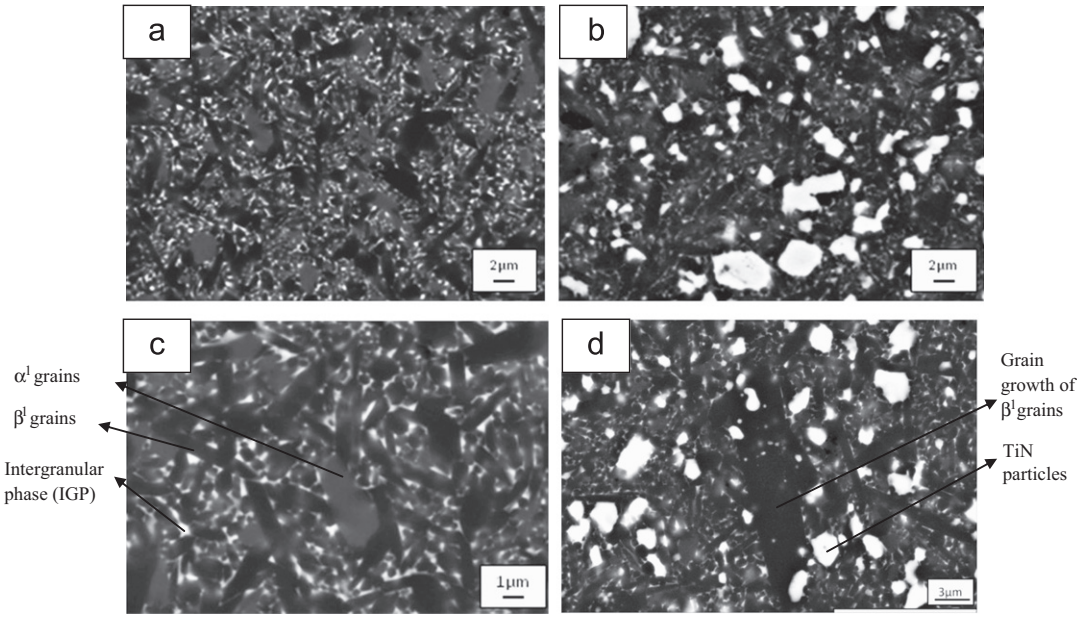

Fig. 2. (a and c) representative back-scattered SEM images of 9Y:0.5Sm:0.5Ca doped SiAlON (z:0.7) and (b and d) SiAlON–TiN composite.

Table 3
Densification behavior of SiAlONs and SiAlON–TiN composites with different intergranular phase contents.

Sample	Aimed z values	Intergranular phase content (mol%)	B.D.	%O.P
YZ2G2 (without TiN)	0.25	2.00	3.2450	0.05
YZ7	0.70	2.50	3.4813	0.09
YZ7G2	0.70	2.00	3.4702	0.11
YZ7G1	0.70	1.50	3.4533	0.24
EZ7	0.70	2.50	3.5812	0.03
EZ7G2	0.70	2.00	3.5520	0.15
EZ7G1	0.70	1.50	3.5086	0.19
YbZ7	0.70	2.50	3.5927	0.08
YbZ7G2	0.70	2.00	3.5699	0.09
YbZ7G1	0.70	1.50	3.5053	0.17
YZ10G3 (without TiN)	1.00	3.30	3.2737	0.23

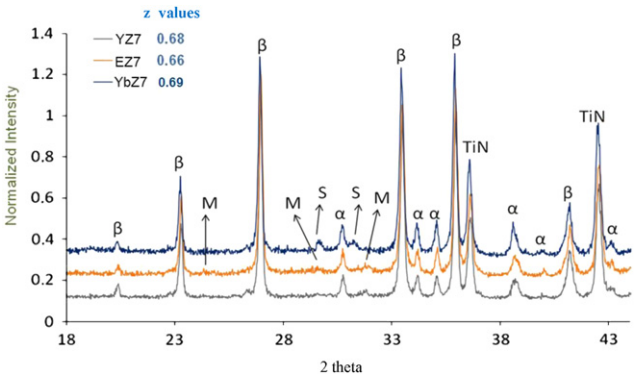

Fig. 3. Comparison of the crystallinity in 9Y/Yb/Er:0.5Sm:0.5Ca containing systems (z:0.7) with 2.5 mol% intergranular phase content (β': beta SiAlON phase, α': alpha SiAlON phase, M': melilite phase ($Ln_2Si_{3-x}Al_xO_{3+x}N_{4-x}$), and S': silicate phase ($Yb_2Si_2O_7$)).

radius increased to 0.8904 Å (for 9Er:0.5Sm:0.5Ca) and 0.9012 Å (for 9Y:0.5Sm:0.5Ca) melilite phase crystallization was obtained. The melilite phase is well known as a good secondary refractory phase which displays good high temperature stability since it has a very high nitrogen content ($Ln_2Si_{(3-x)}Al_xO_{(3+x)}N_{(4-x)}$) [17]. On the other hand, the melting point of $Yb_2Si_2O_7$ phase is high (1850 °C) and is oxidation resistant [33] and it has advantages for high temperature applications. In addition, similar α':β' phase ratios were achieved for all cation systems (see Table 4) due to the approximate values of cation sizes.

Table 4 also presents the relationship between the z value and the cation types of the investigated samples. The results showed that YZ7, EZ7 and YbZ7 samples which have similar z values (0.68, 0.66 and 0.69, respectively) and cation types had no effect on z value for the multi-cation doped samples. Previously, Mandal reported that [34] reduction in z value from 0.78 (Yb with 0.867 Å cation size) to ~0.57 (Sm with 0.964 Å cation size) as ionic radius increases the trends in %α'-SiAlON content and z value could be strongly correlated. However in this used multi-cation doped system, this trend was not observed.

3.3. Effect of IGP content on the z value and the IGP crystallization

The addition of sintering aids results in residual glassy and/or crystalline intergranular phases in the final microstructure. The presence of these phases may downgrade the high temperature properties of final products, and therefore an important target in the development of SiAlON ceramics is to minimize the amount of these phases and to obtain crystalline IGP chemistry instead of glassy phase with fully dense materials.

Table 4
Phase evolution, z values and unitcell dimensions of sintered SiAlON and SiAlON–TiN samples.

Sample	Intergranular phase content (mol%)	Unit cell dimension a-axis (Å)	Unit cell dimension c-axis (Å)	Aimed z value	Measured z value	β':α' ratio (%)	Type of IGP	Cation size(Å)
YZ2G2 (without TiN)	2.00	–	–	0.25	0.23	82β':18α'	M' (s)	0.9012
YZ7	2.50	7.629	2.922	0.70	0.68	81β':19α'	M' (vvw)	0.9012
YZ7G2	2.00	7.630	2.925	0.70	0.75	88β':12α'	A	0.9012
YZ7G1	1.50	7.638	2.927	0.70	0.93	93β':7α'	A	0.9012
EZ7	2.50	7.627	2.923	0.70	0.66	81β':19α'	M' (s)	0.8904
EZ7G2	2.00	7.629	2.924	0.70	0.72	87β':13α'	M' (vw)	0.8904
EZ7G1	1.50	7.630	2.924	0.70	0.72	89β':11α'	A	0.8904
YbZ7	2.50	7.629	2.923	0.70	0.69	81β':19α'	S (vs)	0.8697
YbZ7G2	2.00	7.627	2.925	0.70	0.69	83β':17α'	S (s)	0.8697
YbZ7G1	1.50	7.632	2.925	0.70	0.79	92β':8α'	A	0.8697
YZ10G3 (without TiN)	3.30	7.632	2.926	1.0	0.81	72β':28α'	M' (vs)	0.9329

A: amorphous; M': mellilite; S': silicate; s: strong; vs: very strong; vw: very weak; vvw: very very weak.

In this study, SiAlON compositions were designed with different intergranular phase contents (2.5, 2 and 1.5 mol%). As intergranular phase content decreased at the constant z value (0.7), the bulk densities reduced since the heavy metal (Yb, Er and Y) content was lowered (see Table 3). Open porosities showed an increasing trend with the decrease in the sintering additive content, because reduced amount of transient liquid phase during sintering led to impaired densification (Table 3). The open porosity level of YbZ7 was less than that of YZ7 and EZ7 samples. YbZ7G1 had the lowest IGP content (1.5 mol%), had less open porosity level than YZ7 (which had the highest IGP content of 2.5 mol%). It is evident that Yb doped SiAlONs had better densification behavior after the application of a two step sintering regime.

Figs. 4–8 show the phase relationship of SiAlON–TiN composites which contain different amounts of intergranular phase. The results showed that with the decrease of sintering additive content, the desired α' content was not formed in all the compositions due to the insufficient amount of cation to stabilize the α' phase. For example, the YZ7 sample with 2.5 mol% sintering aid exhibited 81β':19α' phase ratios; however, when the sintering additive content is further reduced to 2 and 1.5 mol%, the β'-phase increased to 88 and 93, respectively. The reason for increased amount of β' can be attributed to the reduction of sintering additive content. This is consistent with Hermann's work, where the α' content was lower than it should be with decreasing sintering additive content [35].

Also crystallization of intergranular phase was inhibited with the reduction of sintering additive content. An amorphous intergranular phase is observed for the samples YZ7G1 and YZ7G2 which contain 1.5 and 2 mol% of intergranular phase, respectively. However, a trace amount of melilite phase was detected for YZ7 sample which also contains a higher intergranular phase content (2.5 mol%).

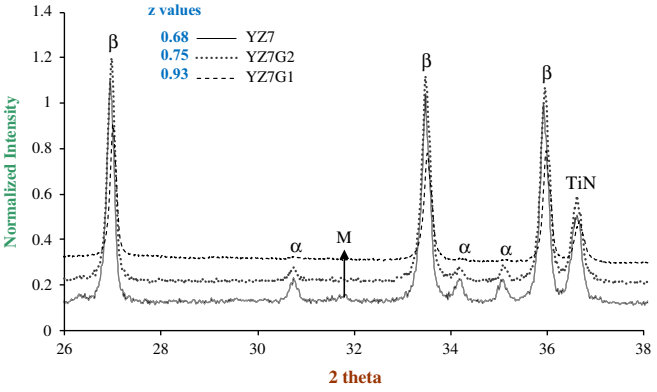

Fig. 4. XRD pattern of 9Y:0.5Sm:0.5Ca containing SiAlON–TiN compositions (z:0.7) which have different amounts of intergranular phase (β':beta SiAlON phase, α':alpha SiAlON phase, M': melilite phase ($Ln_2Si_{3-x}Al_xO_{3+x}N_{4-x}$)).

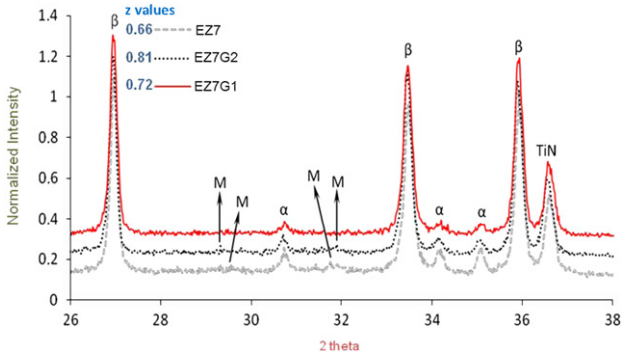

Fig. 5. XRD pattern of 9Er:0.5Sm:0.5Ca containing SiAlON–TiN compositions (z:0.7) which have different amounts of intergranular phase (β':beta SiAlON phase, α':alpha SiAlON phase, and M': Melilite phase ($Ln_2Si_{3-x}Al_xO_{3+x}N_{4-x}$)).

Increase in the sintering additive amount led to phase transformation from amorphous to crystalline melilite for

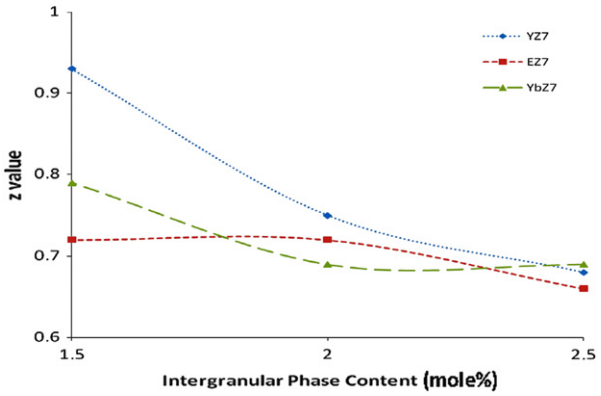

Fig. 6. z value variations for the YZ7, EZ7 and YBZ7 samples which have different intergranular phase contents.

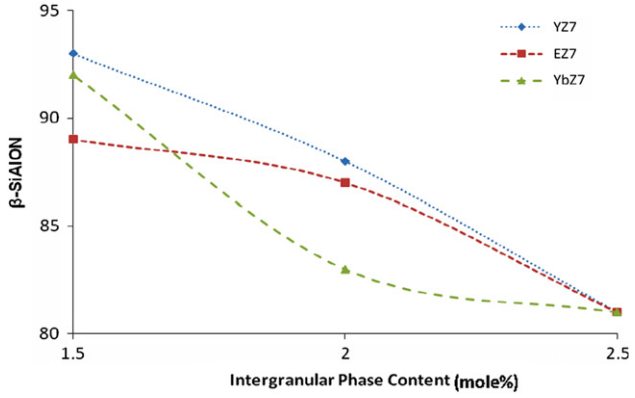

Fig. 7. β'% variations for the YZ7, EZ7 and YBZ7 samples which have different intergranular phase contents.

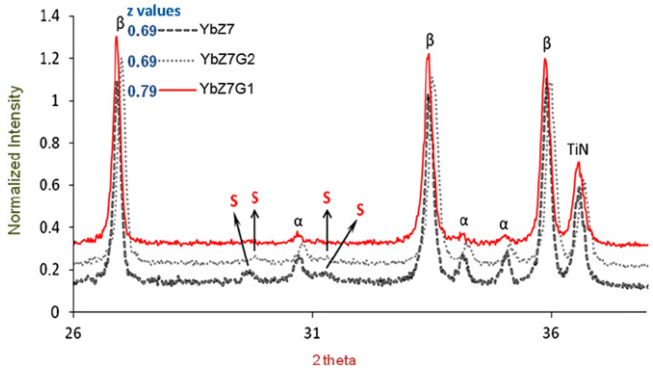

Fig. 8. XRD pattern of 9Yb:0.5Sm:0.5Ca containing SiAlON–TiN compositions (z:0.7) which have different amounts of intergranular phase contents (β': beta SiAlON phase, α': alpha SiAlON phase, and M': melilite phase ($Ln_2Si_{3-x}Al_xO_{3+x}N_{4-x}$)).

the Y doped sample (Fig. 5). As previously mentioned, crystallization tendency of Er and Yb cation was higher than that of Y cation. Therefore, even with a decrease in sintering aid content to 2 mol%, melilite and silicate peaks were present for EZ7G2 and YbZ7G2 samples. Amorphous intergranular phase chemistry was noticed for both the EZ7G1 and YbZ7G1 samples when sintering aid content is reduced to 1.5 mol%.

Another important aspect of present investigation is the effect of intergranular phase amount on z value. With a decrease in sintering additive amount from 2.5 to 2 and 1.5% mole, z value increased from 0.68 to 0.75 and 0.93, respectively, subsequently for Y doped samples (Fig. 6). It is evident that unit cell parameters (a and c axis) increased by the decrease in sintering additive amount (see Table 4). It indicates that more Al and O substituted into β' crystal structure as the sintering additive amount is decreased. The crystal structure expands more as the silicon was replaced by aluminum and nitrogen by oxygen. On the other hand, α' phase was not stable due to higher ionic size of Y than those of Yb and Er. Based on TEM analysis, Yurdakul et al. [36] reported that Yb could be absorbed into a new interstitial site of the β' lattice. Possibly the Y cation preferably substituted in to β' crystal structure instead of α' crystal structure due to bigger cation size. Therefore, β' content reached 93% for YZ7G1 from 81% for YZ7 with decreasing sintering aid amount to 40% (Fig. 7). Also with a decrease in sintering aid amount to ~20%, intergranular phase structure changes from melilite to amorphous. A similar phenomenon was observed for Er-doped samples. From Fig. 7, it can be observed that with the decrease in the IGP content the z value increase is more for Y containing samples than the Er containing samples. On the other hand melilite peaks were still observed for EZ7G2, with the amorphous intergranular phase for YZ7G2. The intensity of melilite peaks decreased with decreasing sintering aid content and increasing z value from 0.66 to 0.72. Although EZ7G1and EZ7G2 had similar z values and α':β' phase ratios, the former contained an intergranular phase which is amorphous and less in quantity while the latter contained a crystalline intergranular phase and higher in quantity.

However, Yb doped samples showed different trends for both Er and Y doped samples in the sense that with a decreasing IGP content z value, α' phase stability and intergranular phase crystallization increased (Figs. 6–8). This may be related to cation sizes as well. The small ionic size of Yb provided more stability of α' phase and higher crystallization tendency of the intergranular phase with lower intergranular phase amount. In the ytterbium based system, the extension of the α-SiAlON region was significantly larger. Yb doped samples showed a trend similar to that of Er doped samples as could be explained by IGP content and crystallization relationship. Crystalline intergranular phase chemistry was achieved even with 2 mol% IGP content sample but its crystalline phase content was higher than that of Er doped sample.

The YZ10G3 sample had the highest (3.3 mol%) intergranular phase amount. Fig. 9 reveals that the sample has both a high z value (0.8) and more melilite phase crystallization due to its higher sintering additive amount (0.33 mol%). IGP crystallization could be controlled by the cation system and cation mole ratios besides intergranular phase content. The YZ10G3 sample exhibits both higher intergranular phase content (3.3 mol%), and highest Sm cation mole ratio.

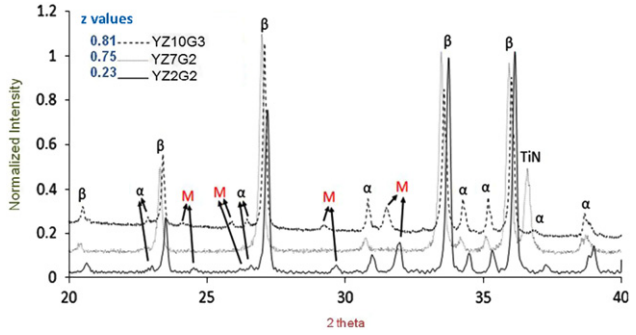

Fig. 9. Comparison of the crystallinity in Y:Sm:Ca containing system with different cation molar ratios and intergranular phase contents (β': beta SiAlON phase, α': alpha SiAlON phase, and M': melilite phase ($Ln_2Si_{3-x}Al_xO_{3+x}N_{4-x}$)).

3.4. The effect of cation ratios on the z value and the IGP crystallization

Our preliminary studies had shown that it was not possible to produce high z value ($z > 0.5$) SiAlONs with crystalline intergranular phase chemistry. In that case, SiAlON compositions were designed with z values of 0.25 and 0.7, same α':β' phase ratio and cation system (9Y:0.5Sm:0.5 Ca). The XRD analysis (Fig. 9) revealed that melilite phase was the product from crystallization of grain boundary phase of the YZ2G2 ($z=0.23$) sample, and it disappeared with the increasing of Al replacement for Si in the YZ7G2 sample and amorphous intergranular phase was obtained as the z value increased to 0.75.

The YZ10G3 sample had the highest (3.3 mol%) intergranular phase content and was rich in Sm and Y cations (4.5Y:4.5Sm:1Ca). Increase in Sm content provided more melilite phase crystallization. Our previous research showed that with an increase in Sm content in the Y–Sm–Ca system, from 5 to 60 mol%, very intense melilite phase crystallization was achieved even after fast cooling because of the lower eutectic temperature of system and high nitrogen solubility in the Sm–Si–Al–O–N system [37]. Zhang et al. [38] reported that Samarium phase relationships with Si–Al–O–N were slightly different from those in the Y–Si–Al–O–N. In the Sm_2O_3–Si_3N_4–AlN–Al_2O_3 system, $SmAlO_3$ and M' phase (melilite solid solution, $Sm_2Si_{(3-x)}Al_xO_{(3+x)}N_{(4-x)}$, $x=0\rightarrow1.0$) were the only two important phases which had tie lines joined to β'-SiAlON and AlN polytypoid phases. M phase coexisted with α' SiAlON. Therefore, Sm SiAlONs had been kinetically favoured in the formation of melilite phase over α'-SiAlON formation.

Thus the YZ10G3 sample had both high z value (0.8) and intense melilite phase crystallization due to the higher (0.33 mol%) sintering additive content, and Sm rich cation system.

3.5. Mechanical properties

Fracture toughness of the SiAlONs was measured by the Vickers indentation technique. The Vickers indents were analyzed by SEM in order to study the indentation cracking behavior. Both indent diagonals and crack lengths around the indentations were measured from the optical microscopy and are given in Table 5. The hardness and fracture toughness of the SiAlON ceramics are summarized in Table 5. From Table 5, it is clear that l/a ratio varies between 1.69 and 2.38 and such values indicate good crack growth resistance property of the investigated ceramics. The differences in microstructure and mechanical properties can be explained on the basis of differences in cation systems and intergranular phase content.

The hardness of SiAlON ceramics depends on phase content and microstructure (porosity, grain size, shape and orientations, second phase (s), z value, etc.). The grain size of SiAlON in high z value (z:4) is 5–10 times larger than that of low z value ($z < 0.5$) SiAlONs. Therefore the hardness values of SiAlONs narrowly varying between 15.14 GPa and 16.48 GPa. On the other hand, hardness increases with the amount of α'-SiAlON, because it was determined by the Burgers vector associated with dislocation movement through lattice and along the c axis of α-SiAlON. The larger Burgers vector corresponds to a higher resistance to dislocation motion in the c axis and hence to a higher hardness. Decrease in α'-SiAlON content leads to decrease in hardness values. The amount of intergranular phase content affects the hardness in a negative way. The reduction in hardness values with the decrease in intergranular phase content can be correlated to change in phase assemblage where α'-SiAlON content diminishes due to insufficient content of cation to stabilize α' phase. Among the SiAlONs, YbZ7 has the highest hardness value since it has the highest α' SiAlON phase (19 α), not much high z value (0.69) and silicate type crystalline intergranular phase chemistry. Well developed α'-SiAlON grains also present in the YbZ7 sample that is different from those in other samples (Fig. 11c).

Several fracture toughness mechanisms have been suggested for silicon nitride based ceramics, namely, microcracking, crack bridging and crack deflection [38]. As can be seen in Fig. 10, the EZ7 (which has the lowest z value of 0.66, crystalline intergranular phase chemistry and high aspect ratio grains over 7) exhibited the highest fracture toughness (7.4 MPa $m^{1/2}$) among of all the investigated materials. Grain growth is also an important factor that may influence the fracture toughness since the α'-SiAlON grains split up into smaller grains of β'-SiAlON and grain boundary phase. It provides more complex possibilities for crack deflection and hence increases in fracture toughness. On a similar account, high toughness is also measured in case of EZ7G2 ceramic. In particular, well developed elongated grains in EZ7 and EZ7G2 can lead to more effective crack bridging and deflection (see Figs. 10 and 11b and e). As can be seen from the SEM images, the number and size of the bright areas increase as the amount of intergranular phase content is increased (see Fig. 11). Decrease in amount of the intergranular phase may lead to stronger interfacial properties and hence lower fracture toughness. This trend was observed in some compositions

Table 5
Mechanical properties and phase evolution of SiAlON–TiN composites.

Sample	*HV*10 (GPa)	*Kc* (MPa $m^{1/2}$)	*c*/*a*	*l*/*a*	*z* value	β′:α′ ratio (%)
YZ7	15.88 ± 0.21	6.4 ± 0.34	1.94	2.06	0.68	81β′:19α′
YZ7G2	15.94 ± 0.18	6.8 ± 0.08	2.00	2.27	0.75	88β′:12α′
YZ7G1	15.58 ± 0.14	6.8 ± 0.10	2.08	2.31	0.93	93β′:7α′
EZ7	15.37 ± 0.09	7.4 ± 0.05	1.85	1.69	0.66	81β′:19α′
EZ7G2	15.16 ± 0.11	7.2 ± 0.15	1.89	1.78	0.72	87β′:13α′
EZ7G1	15.14 ± 0.14	6.4 ± 0.23	2.00	2.27	0.72	89β′:11α′
YbZ7	16.48 ± 0.06	7.0 ± 0.14	2.07	2.30	0.69	81β′:19α′
YbZ7G2	16.12 ± 0.18	6.5 ± 0.03	2.11	2.38	0.69	83β′:17α′
YbZ7G1	15.86 ± 0.11	7.2 ± 0.18	2.00	2.08	0.79	92β′:8α′

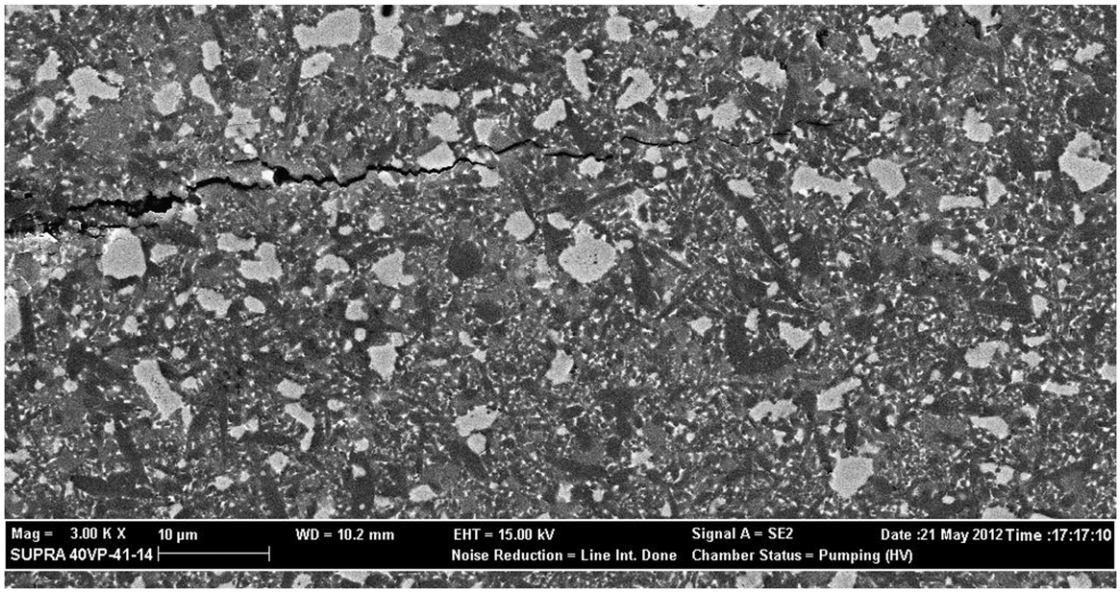

Fig. 10. SEM topography image of the Vickers indentation-induced radial crack pattern of the EZ7 sample.

especially with the decrease in intergranular phase content ~40%, but it was not the case for all (see Table 5).

On the other hand, due to thermal expansion coefficient mismatch between the SiAlON matrix (3×10^{-6}/°C) and TiN (9.4×10^{-6}/°C), extensive microcracking around the TiN particles is inevitable. Absorbed energy by the microcracking could also be another major mechanism for the observed improvement in toughness of the composite materials [39,40]. However extensive microcracking may impair strength properties. Extensive microcracking can be prevented by cooling slowly after sintering. Fangfang et al. observed that a lower sintering temperature would be more suitable technique in order to decrease the thermal mismatch between SiAlON and TiN during the cooling of the composite material as it resulted in decrease in the microcrack density [39].

4. Conclusions

In this article, the effects of cation types, intergranular phase amount and cation mole ratio on the *z* value and the IGP crystallization of SiAlON–TiN composites were systematically investigated. Besides the effect of TiN on densification, phase assemblage and microstructural evolution were determined. Based on the experimental results and observations, the following conclusions were drawn:

1. TiN addition did not have any adverse effect on densification, phase assemblage, *z* value and IGP crystallization.
2. All the SiAlON–TiN composites which contained different types of cations but had the same amount of intergranular phase exhibited similar *z* values. The present results revealed that cation types had no considerable effect on *z* value. An important result was the relationship between cation size and intergranular phase crystallization. Crystallization tendency of Er and Yb cations was higher than that of Y cation.
3. Sintering additive amount influences the α′-SiAlON phase stability, nature of intergranular phase (amorphous or crystalline) and *z* value. The decrease in sintering additive amount resulted in higher β′ phase content and *z* value; crystallization tendency of intergranular phase worsened.

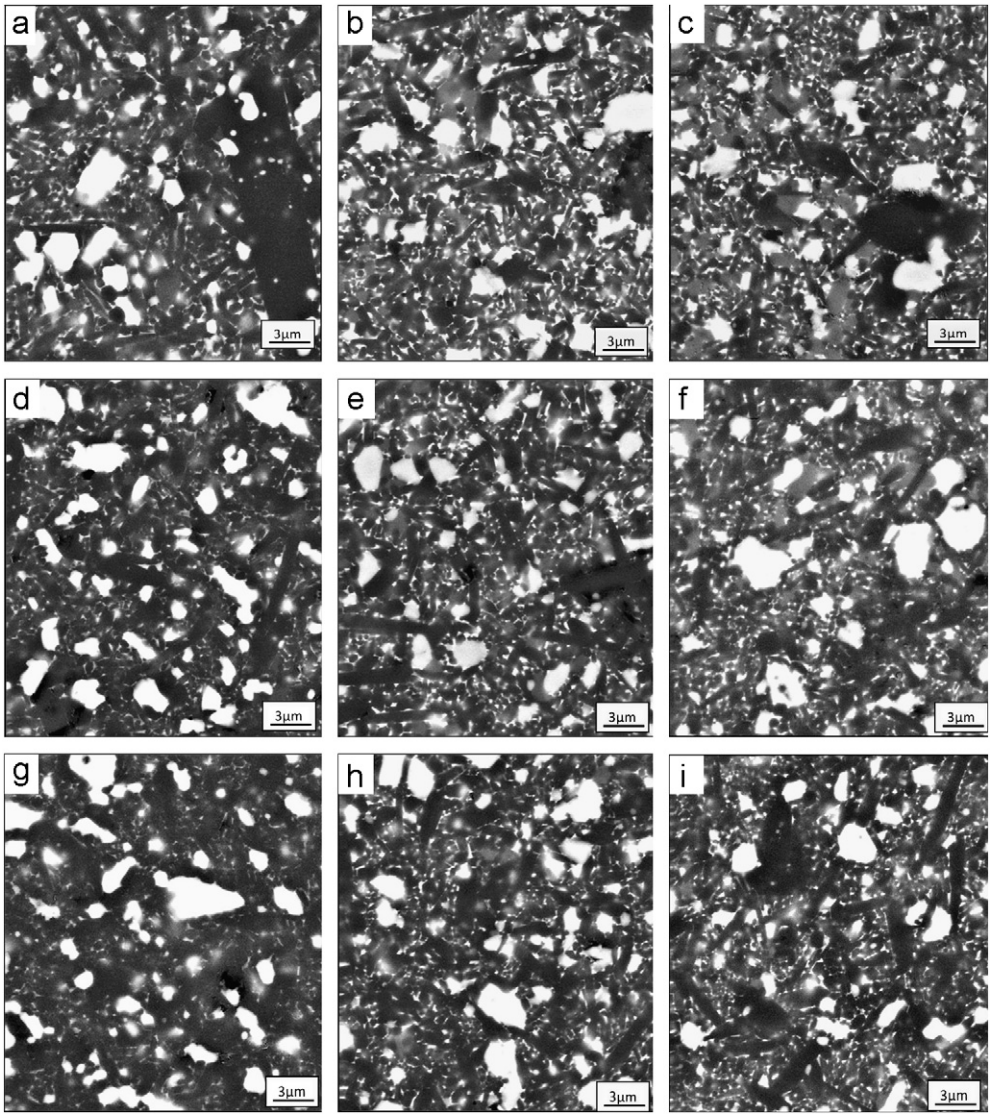

Fig. 11. Representative BSE image of (a) YZ7, (b) EZ7, (c) YbZ7, (d) YZ7G2, (e) EZ7G2, (f) YbZ7G2, (g) YZ7G1, (h) EZ7G1, and (ı) YbZ7G1.

4. It was possible to obtain high z value SiAlONs with an increased Sm cation ratio. This also caused the formation of higher melilite phase crystallization.
5. The z value of SiAlONs changed wuth the intergranular phase amount. The intergranular phase crystallization could be controlled by the cation system, cation mole ratios and intergranular phase content.
6. A combination of hardness of around 15.37 GPa and indentation toughness of 7.4 M $Pam^{1/2}$ could be obtained in the EZ7 sample. This phenomenon is attributed to the more elongated grain morphology and α' phase stability.

Acknowledgments

This work was financially supported by TUBITAK (Ankara, Turkey) in the scope of CAREER-110M727 Project. The authors specially thank Prof. Dr. Ferhat Kara from Anadolu University for his invaluable discussions and Anadolu University, Department of Materials Science and Engineering for allowing us to access his laboratory facilities.

References

[1] G. Blugan, M. Hadad, J. Janczak-Rusch, J. Kuebler, T. Graule, Fractography, mechanical properties, and microstructure of commercial silicon nitride–titanium nitride composites, Journal of the American Ceramic Society 88 (4) (2005) 926–933.
[2] M. Lee, Y. Xiao, D.E. Wittmer, Residual stresses in particle-reinforced ceramic composites using synchrotron radiation, Journal of Materials Science 37 (2002) 4437–4443.
[3] A. Bellosi, A. Fiegna, A. Giachello, P.P. Demaestri, Microstructure and Properties of Electrically Conductive Si_3N_4–TiN Composites. in: Advanced Structural Inorganic Composites, P. Vincenzini, Elsevier Science, Amsterdam, Netherlands, 1991.
[4] R.J. Lumby, R.R. Wills, R.F. Horsley, Method of Forming Ceramic Products, US Patent No. 3,991,148, 1976.
[5] G. Brandt, Wear and Thermal Shock Resistant SiAlON Cutting Tool Material, US Patent No. 5,965,471, 1999.

[6] P. Pettersson, Z. Shen, M. Johnsson, M. Nygren, Thermal shock properties of β-SiAlON ceramics, Journal of the European Ceramic Society 22 (2002) 1357–1365.
[7] S. Hayama, T. Nasu, M. Ozawa, S. Suzuki, Mechanical properties and microstructure of reaction sintered β′-SiAlON ceramics prepared by a slip casting method, Journal of Materials Science 32 (1997) 4973–4977.
[8] B. Basu, R. Kumar, N. Calis Acikbas, F. Kara, H. Mandal, Microstructure–mechanical properties–wear resistance relationship of SiAlON ceramics, Metallurgical and Materials Transactions A 40 (10) (2009) 2319–2332.
[9] Mehrotra, Pankaj, Kumar., High Z SiAlON and Cutting Tools Made Therefrom and Method of Using, International Application Published Under the Patent Cooperation Treaty (PCT), WO 94/12317, 9 06 1994.
[10] R.L. Yeckley, B. North, Ceramic Material and Method of Manufacture. US Patent No. 4,563,433, 1986.
[11] X. Yi, K. Watanabe, T. Akiyama, Vickers hardness of β-SiAlON prepared by a combination of combustion synthesis and spark plasma sintering, Journal of the Ceramic Society of Japan 118 (3) (2010) 250–252.
[12] R. Ramesh, M.J. Pomeroy, Effect of z value on densification and properties of SiAlON–SiC matrices and composites, Key Engineering Materials 86–87 (1993) 271–278.
[13] J. Mukerji, J. Prakash, Wear of nitrogen ceramics and composites in contact with bearing steel under oscillating sliding condition, Ceramics International 24 (1998) 19–24.
[14] T. Satoh, S. Sakaguchi, K. Hirao, M. Toriyama, S. Kanzaki, Influence of aluminum–oxygen–yttrium solid solution on the aqueous tribological behavior of silicon nitride, Journal of the American Ceramic Society 84 (2) (2001) 462–464.
[15] H. Mandal, F. Kara, S. Turan, A. Kara, Novel SiAlON ceramics for cutting tool applications, Key Engineering Materials 237 (2003) 193–202.
[16] N. Acikbas Calis, A. Kara, S. Turan, F. Kara, H. Mandal, B. Bitterlich, Influence of type of cations on intergranular phase crystallization of SiAlON ceramics, Materials Science Forum 554 (2007) 119–122.
[17] F. Kara, H. Mandal, S. Turan, A. Kara, N. Acikbas Calis, Development strategies for SiAlON ceramics, in: Proceedings of the Global Roadmap for Ceramics ICC2, Verona, Italy, 2008, pp. 119–128.
[18] R.L. Satet, M.J. Hoffmann, Grain growth anisotropy of β-silicon nitride in rare-earth doped oxynitride glasses, Journal of the European Ceramic Society 24 (2004) 3437–3445.
[19] A. Ziegler, C. Kisielowski, M.J. Hoffmann, R.O. Ritchie, Atomic resolution transmission electron microscopy of silicon nitride and the intergranular structure of a Y_2O_3–silicon nitride ceramic, Journal of the American Ceramic Society 86 (10) (2003) 1777–1785.
[20] N. Shibata, S.J. Pennycook, T.R. Gosnell, S.G. Painter, W.A. Shelton, P.F. Becher, Observation of rare-earth segregation in silicon nitride ceramics at subnanometre dimensions, Nature 428 (2004) 730–733.
[21] R.L. Satet, M.J. Hoffmann, Influence of the rare-earth element on the mechanical properties of RE–Mg-bearing silicon nitride, Journal of the American Ceramic Society 88 (9) (2005) 2485–2490.
[22] A. Ziegler, J.C. Idrobo, M.K. Cinibulk, C. Kisielowski, N.D. Browning, R.O. Ritchie, The effect of the crystal–intergranular phase interface on the fracture toughness of silicon nitride ceramics, Science 306 (2004) 1768–1770.
[23] H. Mandal, F. Kara, S. Turan, A. Kara, Multication Doped Alpha–Beta SiAlON Ceramics, US Patent No. 7,064,095 B2, 2002.
[24] K. Liddell, X-ray Analysis of Nitrogen Ceramic Phases, M.Sc. Thesis, University of Newcastle, Tyne, UK, 1979.
[25] A.G. Evans, E.A. Charles, Fracture thoughness determinations by indentation, Journal of the American Ceramic Society 59 (1976) 371–372.
[26] K. Niihara, R. Morena, P.H. Hasselman, Evaluation of Kıc of brittle solids by the indentation method with low crack-to-indent ratios, Journal of Materials Science Letters 1 (1982) 13–16.
[27] R.G. Duan, G. Roebben, J. Vleugels, O. Van Der Biest, Effect of TiX(X=C, N, O) additives on microstructure and properties of silicon nitride based ceramics, Scripta Materialia 53 (2005) 669–673.
[28] T. Ekström, P. Olsson, β-SiAlON ceramics with TiN particle inclusions, Journal of the European Ceramic Society 13 (6) (1994) 551–559.
[29] M. Menon, I-Wei Chen, Reaction densification of α-SiAlON: I, wetting behavior and acid base reactions, Journal of the American Ceramic Society 78 (3) (1995) 545–552.
[30] S.L. Hwang, I.W. Chen, Reaction hot pressing of alpha and beta SiAlON ceramics, Journal of the American Ceramic Society 77 (1) (1994) 165–171.
[31] H. Mandal, D.P. Thompson, T. Ekstrom, Reversible α/β SiAlON transformation in heat-treated SiAlON ceramics, Journal of the European Ceramic Society 12 (1993) 421–429.
[32] H. Mandal, D.P. Thompson, T. Ekstrom, Heat treatment of Ln–Si–Al–O–N glasses, Key Engineering Materials 72–74 (1992) 187–203.
[33] E.M. Levin, C.R. Robbins, H.F. McMurdie, Phase diagrams for ceramists, Journal of the American Ceramic Society (1969) 108.
[34] H. Mandal, Heat-Treatment of SiAlON Ceramics, Ph.D. Thesis, University of Newcastle upon Tyne, UK, 1992.
[35] M. Herrmann, S. Höhn, A. Bales, Kinetics of rare earth incorporation and its role in densification and microstructure formation of α-SiAlON, Journal of the European Ceramic Society 32 (7) (2012) 1313–1319.
[36] H. Yurdakul, J.C. Idrobo, S.J. Pennycook, S. Turan, Towards atomic scale engineering of rare-earth-doped SiAlON ceramics through aberration-corrected scanning transmission electron microscopy, Scripta Materialia 65 (2011) 656–659.
[37] N. Acikbas Calis, H. Yurdakul, H. Mandal, F. Kara, S. Turan, A. Kara, B. Bitterlich, Effect of sintering conditions and heat treatment on the properties, microstructure and machining performance of α:β-SiAlON ceramics, Journal of the European Ceramic Society 32 (2012) 1321–1327.
[38] C. Zhang, W.Y. Sun, D.S. Yan, Optimizing mechanical properties and thermal stability of Ln–α–β–-SiAlON by using duplex Ln elements (Dy and Sm), Journal of the European Ceramic Society 19 (1) (1999) 33–39.
[39] X. Fangfang, S. Wen, L.O. Nordberg, T. Ekstrom, TEM study of Y-doped α-SiAlON composite with 10 vol% TiN particulates, Materials Letters 34 (1998) 248–252.
[40] T. Nagaoka, M. Yasuoka, K. Hirao, S. Kanzaki, Effects of TiN particle size on mechanical properties of Si_3N_4/TiN particulate composites, Journal of the Ceramic Society of Japan 100 (1992) 617–620.